MICROPHYSICS COMPLEXITY EFFECTS ON STORM EVOLUTION AND ELECTRIFICATION

Blake J. Allen
National Weather Center Research Experience For Undergraduates, Norman, Oklahoma and Pittsburg State University, Pittsburg, Kansas

Edward R. Mansell
NOAA / National Severe Storms Laboratory, Norman, Oklahoma

ABSTRACT

Microphysics parameterization schemes used in numerical storm models vary greatly in complexity. One of the ways in which these schemes vary is in the number of microphysical moments that they predict for each of the hydrometeor categories included in the scheme. This study analyzed the effects of enabling prediction of a second microphysical moment, number concentration, for each hydrometeor category in a mixed phase, bulk microphysics scheme. The addition of number concentration prediction for cloud droplets was found to have a large influence on the early development of the simulated storm, while the addition of number concentration prediction for rain was found to have the largest impact on the storm's reflectivity structure. The electrification of the storm was also found to be quite sensitive to changes in the microphysics complexity, due at least in part to variations in cloud ice and graupel production in the different model runs.

1. INTRODUCTION

Microphysics parameterization schemes commonly used in numerical storm models vary in a number of important ways. Among these variations are differences in how hydrometeor size is accounted for between bulk schemes and bin schemes, differences in the types of hydrometeors modeled in warm rain schemes as opposed to mixed phase schemes, and differences in how many microphysical properties are predicted moving from one-moment schemes to multi-moment schemes.

Bin schemes, which treat different hydrometeor size ranges separately, are much more computationally expensive than bulk schemes, which treat the range of hydrometeor sizes together by predicting one or many hydrometeor properties, such as mixing ratio and/or number concentration, for a specified size distribution (Straka and Mansell 2005).

Warm rain schemes and mixed phase schemes differ in that warm rain schemes only include categories for water vapor and liquid hydrometeors, such as cloud droplets and rain, while mixed phase schemes include, in addition to the warm rain categories, various types of frozen hydrometeors, such as cloud ice, snow, graupel, and hail. Mixed phase schemes themselves vary greatly in the number of types of frozen hydrometeors they take into account, ranging from 3-ice schemes such as Lin et al. (1983, hereafter LFO83) and Ziegler (1985) to the 10-ice scheme of Straka and Mansell (2005).

Finally, microphysics parameterizations vary in the number of properties that they predict for each hydrometeor category. One-moment schemes usually only predict the mass mixing ratios for each category, and either set as constant or diagnose other properties of the category's size distribution, such as the intercept, the slope, and the number concentrations. Two-moment schemes, on the other hand, typically predict mixing ratios as well as a second property for each hydrometeor category; most commonly, the second property predicted by these schemes is the number concentration (Straka et al. 2005). The addition of the prediction of a second microphysical moment allows more flexibility for other microphysical properties. For example, in this study, when number concentration is predicted as well as mixing ratio, the size distribution intercept can be diagnosed at each time and grid point rather than being set to a constant value for the entire domain throughout the simulation. In general, predicting additional moments improves the parameterization of physical processes with less computational expense than using a bin scheme.

The inclusion of more complex microphysics parameterizations in numerical storm models is expected to lead to more realistic storm evolution since the dynamics of the storm are heavily influenced by microphysical processes

Model run	Cloud ice # concentration prediction	Cloud droplet # concentration prediction	Rain # concentration prediction	Graupel / snow # concentration prediction
3-o				
3-i	X			
3-id	X	X		
3-idr	X	X	X	
3-idrgs	X	X	X	X

Table 1: Hydrometeor categories with number concentration prediction for each model run.

such as heating and cooling due to phase changes of the water mass contained in the storm. Storm electrification, also, is very dependent on microphysical processes, especially processes involving frozen hydrometeors.

Previous studies have tested the sensitivity of various characteristics of simulated storms to differences in the microphysics parameterization used for the simulation. Ferrier et al. (1995) explored differences between a two-moment, 4-ice scheme, the one-moment, 3-ice LFO83 scheme and a variation of the LFO83 scheme, and the same study tested the sensitivity of the 3-ice schemes to variations in microphysical parameters such as intercept values and fall speeds. Meyers et al. (1997) compared the sensitivity of a one-moment scheme and a two-moment scheme to variations in different microphysical parameters such as the number concentration of cloud droplets and changes in the ice crystal habit. Gilmore et al. (2004a, 2004b) examined the differences in storms simulated using a warm rain scheme and a mixed phase scheme similar to LFO83, and also tested the sensitivity of the mixed phase scheme to variations in intercept values and graupel density.

The purpose of this study was to test, using a mixed phase, bulk microphysics scheme, the sensitivity of a simulated storm to the prediction of number concentration for various hydrometeor types, including cloud ice, cloud droplets, rain, snow, and graupel. Various storm characteristics were analyzed, including the general evolution of the storm as shown by the updraft mass flux, maximum updraft speeds, radar reflectivity, and updraft structure; the microphysical evolution of the storm; and the electrification and lighting production in the storm.

In section 2 of this paper, the numerical storm model used as well as the similarities and differences in the model runs are discussed. Section 3 covers the results of the model runs as well as discussion of the results. Finally, section 4 concludes the paper.

2. METHODOLOGY

This study used the NSSL Collaborative Model for Multiscale Atmospheric Simulation described in Wicker and Wilhelmson (1995) and Coniglio et al. (2006). The model was set to a grid spacing of 400 m in both horizontal directions and a constant grid spacing of 200 m in the vertical direction, with a domain size of 50 km x 50 km in the horizontal directions and 21 km in the vertical direction. The initial conditions for every model run in this study used a sounding similar to the one described in Weisman and Klemp (1984), except with a surface water vapor mixing ratio of 12.5 g kg^{-1}, and a shear profile equivalent to the half circle hodograph with arc length 20 m s^{-1} over a depth of 5 km described in the same paper. The model domain was set to move along with the storm. In each model run, the storm was initiated using an ellipsoidal region of vertical forcing with radii of 6 km in the horizontal directions and 2 km in the vertical direction.

Tests were done using an updated 3-ice microphysics scheme (Ziegler 1985, Zrnic et al. 1993) that was modified to be able to run as a one-moment scheme in addition to its original two-moment configuration. The scheme includes categories for cloud droplets, rain, cloud ice, snow, and graupel. Also, the scheme predicts the bulk density for graupel particles. The electrification scheme used in all model runs was as described in Mansell et al. (2005), and the non-inductive graupel charging in the electrification scheme was based on the laboratory results of Saunders and Peck (1998). The lightning parameterization used produces three dimensional, branched lightning, as described in Mansell et al. (2002).

Five model runs were completed using the 3-ice microphysics scheme, as shown in Table 1. With each run number concentration prediction was turned on for an additional hydrometeor category. In addition to the number concentration prediction variations, in all model runs the hydrometeor mixing ratios were predicted for each hydrometeor type.

3. RESULTS AND DISCUSSION

The overall evolution of updraft cells in each simulation is shown in Figure 1 using the updraft mass flux at the -20°C level (6.7 km). There are only very slight changes in the overall evolution of the storm through 90 minutes caused by enabling number concentration prediction for cloud ice in run 3-i. Upon enabling number concentration prediction for cloud droplets, however, the initial development of the updraft is significantly delayed in run 3-id. Enabling number concentration prediction for additional categories in addition to cloud ice and cloud droplets has smaller effects initially than enabling cloud droplet number concentration prediction, but eventually leads to similar differences in storm evolution after 50-60 minutes. The differences in storm evolution between the runs, especially the change when cloud droplet number concentration prediction is enabled, can again be seen in Figure 2, which compares the maximum updraft velocities for the five 3-ice model runs.

The reason for the delay in updraft development when cloud droplet number concentration is predicted appears to be due to a change in how the microphysics parameterization deals with supersaturation: When cloud droplet number concentration is not predicted, the model does not allow supersaturation with respect to liquid; rather, if a grid point is found to have a water vapor value higher than that required for saturation, the model condenses water vapor until 100% water saturation is reached, or, in the presence of cloud ice, until a weighted saturation is reached. When cloud droplet number concentration is predicted, however, the model allows supersaturation to persist and evolve more realistically. This reasoning is supported by Figure 3, which shows that the development of cloud droplet mass is delayed in a manner similar to that of the updraft development when cloud droplet number concentration prediction is enabled. This delay in the development of cloud droplet mass in turn delays the release of latent heat associated with the condensation of the water vapor and thus keeps the updraft from developing as early as in model runs 3-o and 3-i.

The surface radar reflectivity as well as the updraft velocities at the -20°C level are shown for 42 minutes in Figure 4 and for 70 minutes in Figure 5. Run 3-i is nearly identical to the full one moment run 3-o and is thus omitted from these two figures. Although the updraft velocities have a similar structure and position for all model runs at 42 minutes, the reflectivity at this time, soon after precipitation first reaches the ground, is shifted significantly to the east in the 3-idr and 3-idrgs runs. The similarity between the 3-i and 3-id runs at this point was somewhat unexpected considering the differences in the early updraft evolution; however, there are some other similarities between the 3-o and 3-id runs, such as the rain mass for the 3-id run being somewhat more similar to the rain mass in the 3-i and 3-o runs than to the 3-idr and 3-idrgs runs early in the simulation, as can be seen in Figure 6. The cause for the shift in the location of the surface precipitation between runs 3-id and 3-idr may be due to differences in raindrop size between the two model runs. When number concentration is predicted for rain, graupel melting to rain creates larger drops, while when number concentration is not predicted for rain, graupel melting to rain is handled differently and produces smaller drops with lower fall speeds that are carried further to the west by winds within 2 km of the surface.

At 70 minutes, the reflectivity and updraft velocity structures are still mostly similar for the 3-o and 3-id runs (Figure 5); also, the 3-idr and 3-idrgs runs are again different from the 3-o and 3-id runs, but by this time these runs have also become more different from each other than at 42 minutes, with the precipitation at the surface concentrated nearer the updraft in the 3-idr run than in the 3-idrgs run. The updraft is also somewhat weaker and slightly narrower in the 3-idrgs run, consistent with what could be expected from the smaller updraft mass flux for run 3-idrgs at 70 minutes shown in Figure 1. Even though the similarity between the 3-o and the 3-id runs persists at this time, the difference in the rain mass between the runs has increased.

The overall storm electrification for each 3-ice model run is shown in Figure 7 by the amount of charge discharged via intracloud lightning flashes. Although the timing of the updraft development in the 3-o run and the 3-i run is essentially identical, there is a delay in the electrification of the storm in the 3-o run. A factor that most likely makes a major contribution to this difference is the apparent distribution of the cloud ice mass among a larger number of smaller cloud ice particles in the 3-i run compared to a smaller number of larger particles in the 3-o run. The differences in cloud ice number concentration and charge separation rate between the two model runs around the time that the storm first becomes electrified enough to produce lightning (at t = 30 minutes) can be seen in Figure 8.

The differences in the timing of the initial electrification for the 3-id, 3-idr, and 3-idrgs runs are likely due to delays in the initial development

of graupel (see Figure 9) in the 3-idr and 3-idrgs runs relative to the 3-id run, while the delay in electrification between the 3-i and 3-id runs is likely simply due to the delayed updraft development in the 3-id run.

Specific causes for the variations in storm electrification between model runs at times beyond 45-50 minutes are somewhat more difficult to determine, since the differences are due in part to changes in the overall storm evolution and in part to changes in the microphysical evolution. However, some differences should be noted. The weaker electrification of the full two-moment (3-idrgs) run is likely due at least in part to the significantly smaller amounts of cloud ice present throughout that model run, as shown in Figure 10. A major cause of the lower amounts of cloud ice in the 3-idrgs run appears to be the conversion of cloud ice to snow -- the 3-idrgs run has a significantly larger amount of snow mass than the other model runs, as can be seen in Figure 11. Slightly lower amounts of graupel mass in the 3-idrgs run during most of the simulation, as shown in Figure 9, may also contribute to the weaker electrification of the storm in this run. The differences in cloud ice and graupel mass for the 3-idrgs storm may in turn be partly a result of that simulated storm being slightly weaker overall than the rest of the storms during a large part of the time simulated, at least in terms of the updraft mass flux and maximum updraft velocity (Figures 1 and 2). In addition to the lower amount of graupel mass in the 3-idrgs run, the graupel present in that storm may be smaller and thus have lower fall speeds than in the other storms, which would also slow the rate of charge separation and lessen the magnitude of the electrification in that model run. The 3-o run also continues to have weaker electrification than the 3-i run throughout the simulated time. Since the 3-o and 3-i runs have nearly identical overall evolution, the electrification differences must be due to variations in the microphysical evolution of the storms, and it can be seen from Figure 8 that the 3-o run has a smaller amount of cloud ice mass than the 3-i run during the entire simulation. In addition to the lower overall amount of cloud ice mass in the 3-o run, the difference in the cloud ice number concentration between the 3-o and 3-i runs present at 30 minutes persists as the cloud ice mass in the 3-o run continues to be distributed among a smaller number of larger ice crystals than in the 3-i run throughout the simulation (Figure 12 shows this at t = 70 minutes).

4. CONCLUSIONS

The initial updraft development in the simulated storms appeared to be most sensitive to cloud droplet number concentration prediction, which was most likely due to a change in how the model handles supersaturation when cloud droplet number concentration prediction is enabled. Enabling number concentration prediction for additional hydrometeor categories beyond cloud droplets tended to delay the development of cloud ice and graupel, even though the initial timing of the updraft development for each of the 3-id, 3-idr, and 3-idrgs runs was similar. Unlike the early updraft mass flux development, the surface radar reflectivity was, both early and late in the simulation, altered the most by enabling the prediction of rain number concentration. Electrification of the simulated storms varied greatly between the various model runs, with differences in the development of graupel and cloud ice as well as differences in the overall evolution of the storms having effects on this aspect of the storm.

A number of additional tests could be done to extend this work in the future. First, it would be useful to attempt to simulate an observed storm to see if the full two-moment version of the microphysics scheme can in fact reproduce the observed storm better than the less complex versions of the scheme, as expected. It could also be informative to run tests similar to those done in this study except using storms simulated with different soundings and shear profiles to see if those storms have variations in their development similar to those of the storms studied here. Another test that could be useful would be to enable number concentration prediction for each hydrometeor category individually instead of progressively enabling number concentration prediction for more categories as was done here. This could allow the determination of whether or not enabling number concentration prediction only for certain hydrometeor categories could give results similar to the model run where number concentration is predicted for all hydrometeor categories.

ACKNOWLEDGEMENTS

This material is based upon work supported by the National Science Foundation under Grant No. ATM-0648566. Any opinions, findings, and conclusions or recommendations expressed in this material are those of the authors and do not necessarily reflect the views of the National Science Foundation. Support was also provided by the National Severe Storms

Laboratory and National Science Foundation grant ATM-0451639. Funding for this research also was provided under NOAA-Univ. of Oklahoma Cooperative Agreement NA17RJ1227. The authors would like to thank Daphne Ladue for all of her work organizing and directing the National Weather Center REU.

REFERENCES

Coniglio, M. C., D. J. Stensrud, and L. J. Wicker, 2006: Effects of upper-level shear on the structure and maintenance of strong quasi-linear mesoscale convective systems. *J. Atmos. Sci.*, **63**, 1231–1252.

Ferrier, B. S., W.-K. Tao, and J. Simpson, 1995: A double-moment multiple-phase four-class bulk ice scheme. Part II: Simulations of convective storms in different large-scale environments and comparisons with other bulk parameterizations. *J. Atmos. Sci.*, **52**, 1001–1033.

Gilmore, M. S., J. M. Straka, and E. N. Rasmussen, 2004a: Precipitation uncertainty due to variations in precipitation particle parameters within a simple microphysics scheme. *Mon. Wea. Rev.*, **132**, 2610–2627.

— 2004b: Precipitation uncertainty due to variations in precipitation particle parameters within a simple microphysics scheme. *Mon. Wea. Rev.*, **132**, 2610–2627.

Lin, Y.-L., R. D. Farley, and H. D. Orville, 1983: Bulk parameterization of the snow field in a cloud model. *J. Climate Appl. Meteor.*, **22**, 1065–1089.

Mansell, E. R., D. R. MacGorman, C. L. Ziegler, and J. M. Straka, 2002: Simulated three-dimensional branched lightning in a numerical thunderstorm model. *J. Geophys. Res.*, **107**, doi:10.1029/2000JD000244.

—2005: Charge structure and lightning sensitivity in a simulated multicell thunderstorm. *J. Geophys. Res.*, **110**, doi:10.1029/2004JD005287.

Meyers, M. P., R. L. Walko, J. Y. Harrington, and W. R. Cotton, 1997: New RAMS cloud microphysics parameterization. Part II: The two-moment scheme. *Atmos. Res.*, **45**, 3–39.

Saunders, C. P. R. and S. L. Peck, 1998: Laboratory studies of the influence of the rime accretion rate on charge transfer during crystal/graupel collisions. *J. Geophys. Res.*, **103**, 13949–13956.

Straka, J. M., M. S. Gilmore, K. M. Kanak, and E. N. Rasmussen, 2005: A comparison of the conservation of number concentration for the continuous collection and vapor diffusion growth equations using one- and two-moment schemes. J. Appl. Meteor., **44**, 1844-1849.

Straka, J. M. and E. R. Mansell, 2005: A bulk microphysics parameterization with multiple ice precipitation categories. *J. Appl. Meteor.*, **44**, 445–466.

Weisman, M. L. and J. B. Klemp, 1984: The structure and classification of numerically simulated convective storms in directionally varying wind shears. *Mon. Wea. Rev.*, **112**, 2479–2498.

Wicker, L. J. and R. B. Wilhelmson, 1995: Simulation and analysis of tornado development and decay within a three-dimensional supercell thunderstorm. *J. Atmos. Sci.*, **52**, 2675–2703.

Ziegler, C. L., 1985: Retrieval of thermal and microphysical variables in observed convective storms. Part I: Model development and preliminary testing. *J. Atmos. Sci.*, **42**, 1487–1509.

Zrnic, D. S., N. Balakrishnan, C. L. Ziegler, V. N. Bringi, K. Aydin, and T. Matejka, 1993: Polarimetric signatures in the stratiform region of a mesoscale convective system. *J. Appl. Meteor.*, **32**, 678–693.

FIGURES

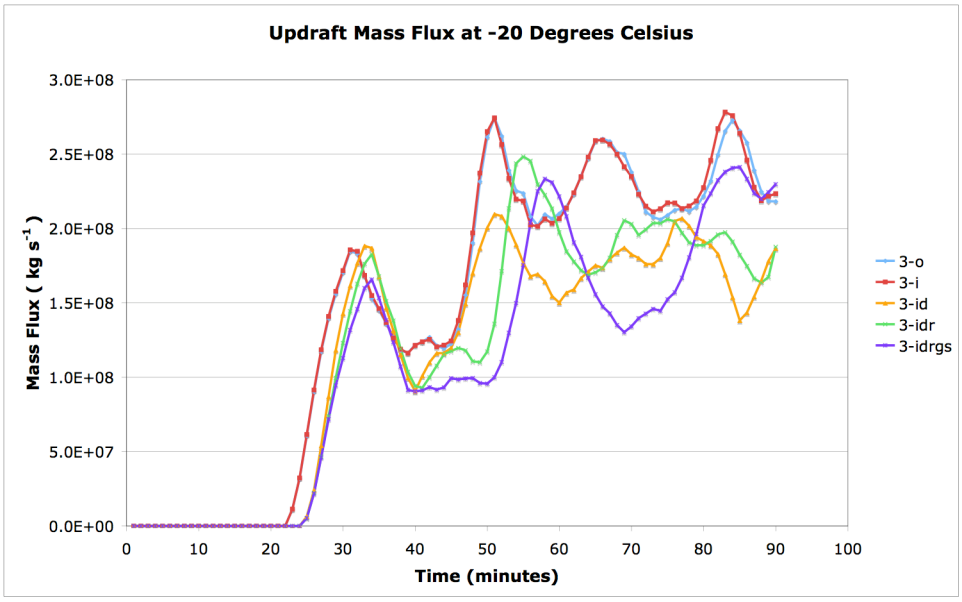

Figure 1: Updraft mass flux integrated over the -20°C temperature level (6.7 km) vs. time. Each line corresponds a model run as shown in the legend on the right.

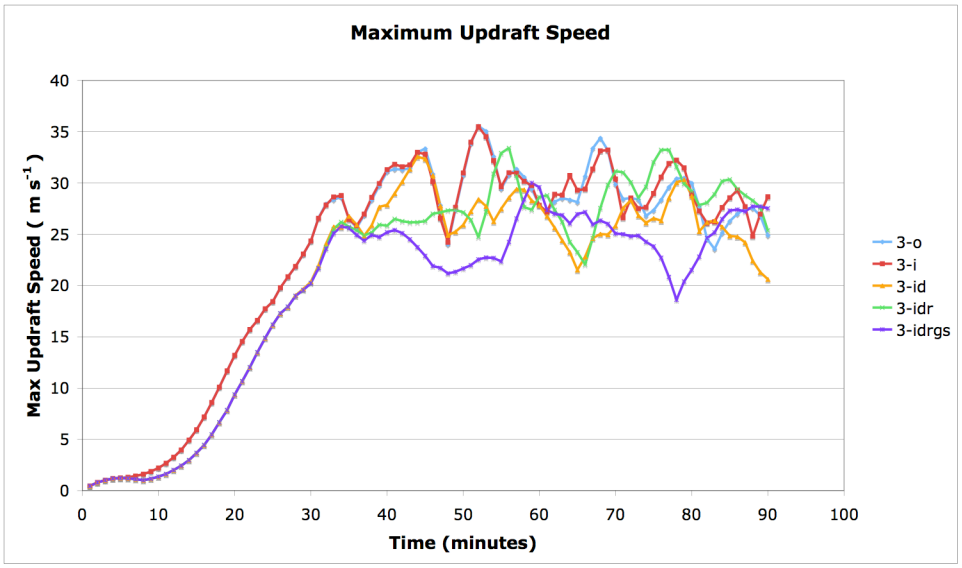

Figure 2: Maximum updraft speed within the model domain.

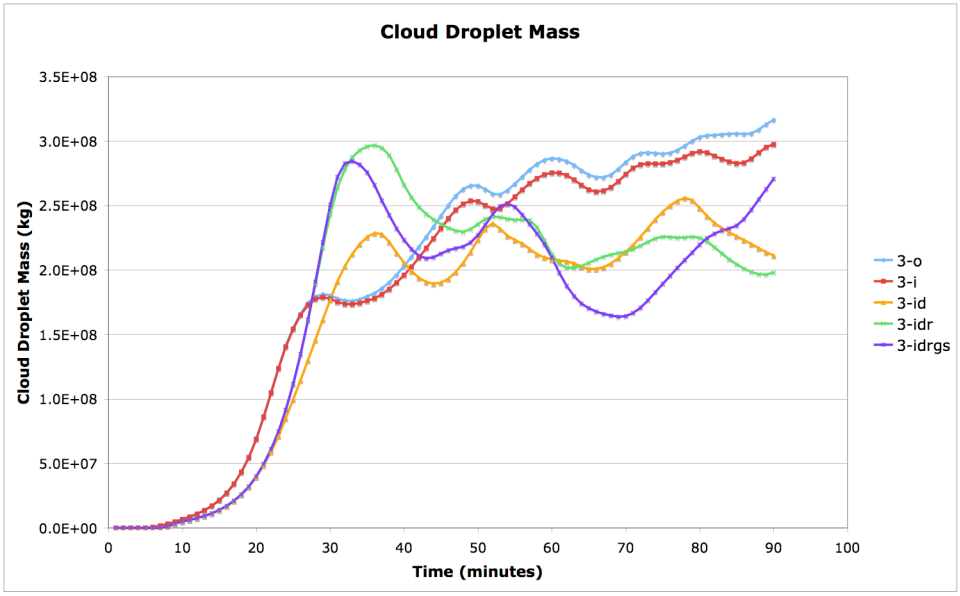

Figure 3: Total cloud droplet mass within the model domain.

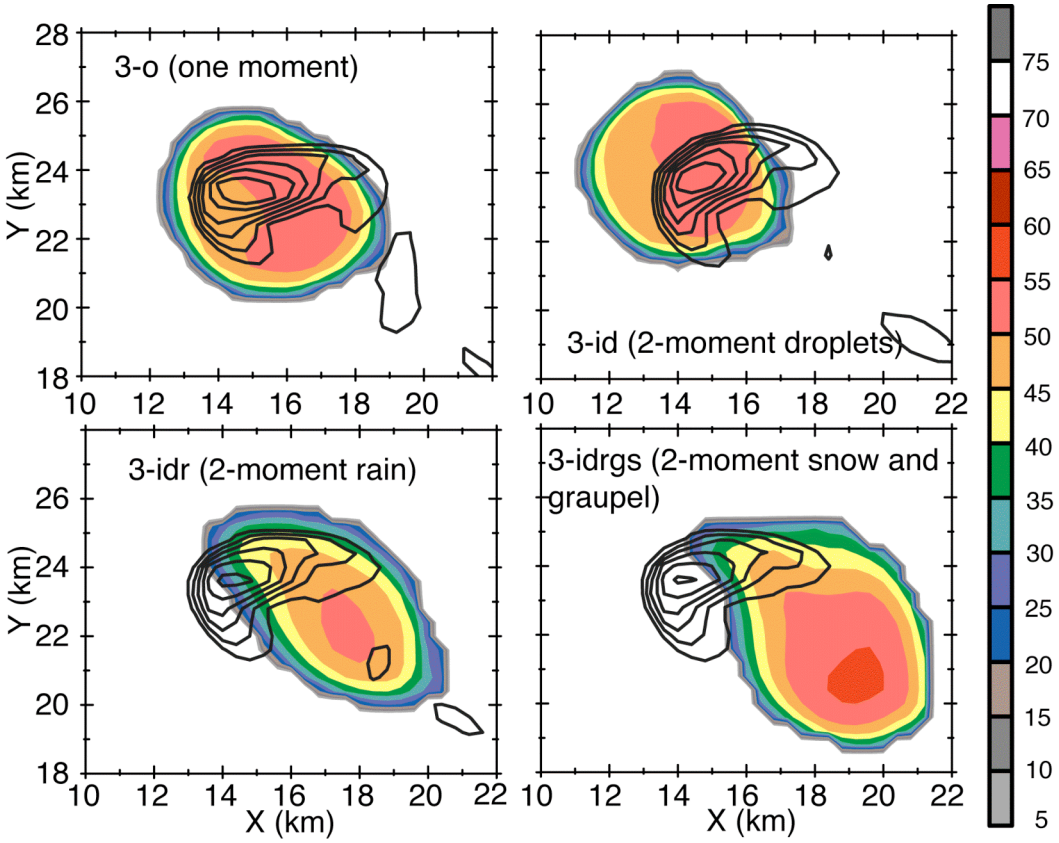

Figure 4: Surface radar reflectivity (filled contours) and -20°C (6.7 km) updraft speed (black lines) at 42 minutes. The contour interval for the updraft speed is 4 m s^{-1}.

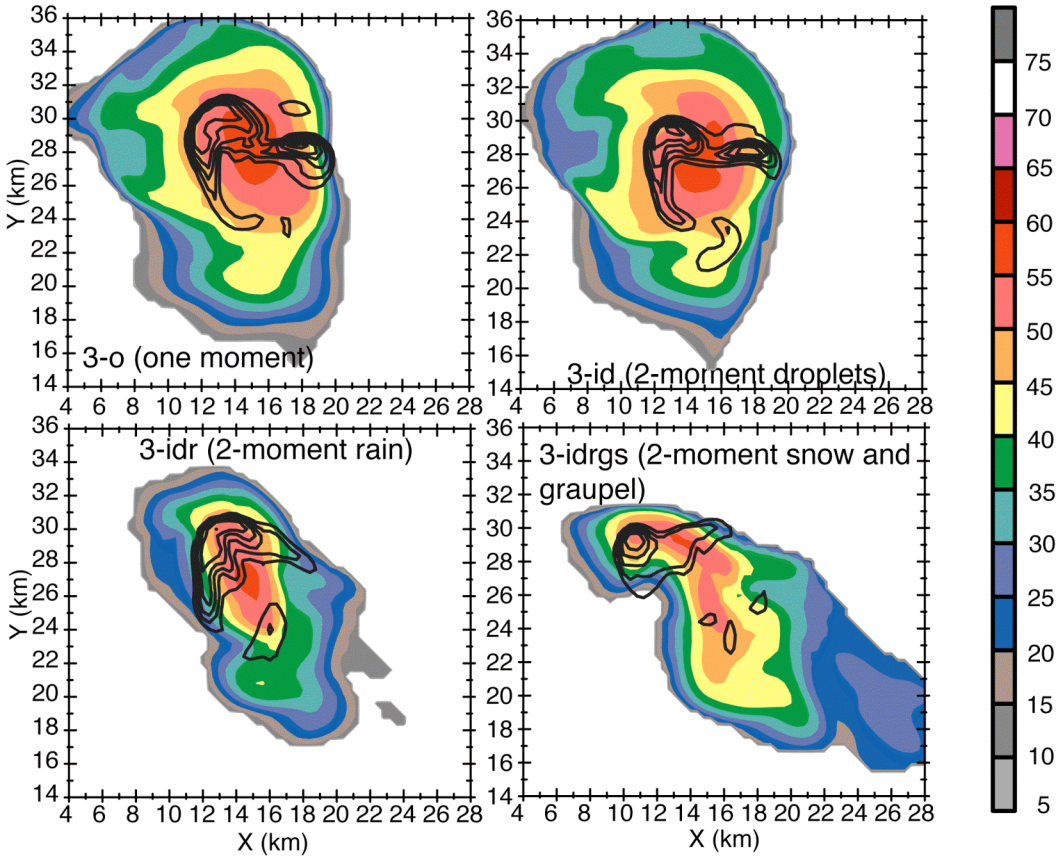

Figure 5: As in Figure 4 except at 70 minutes.

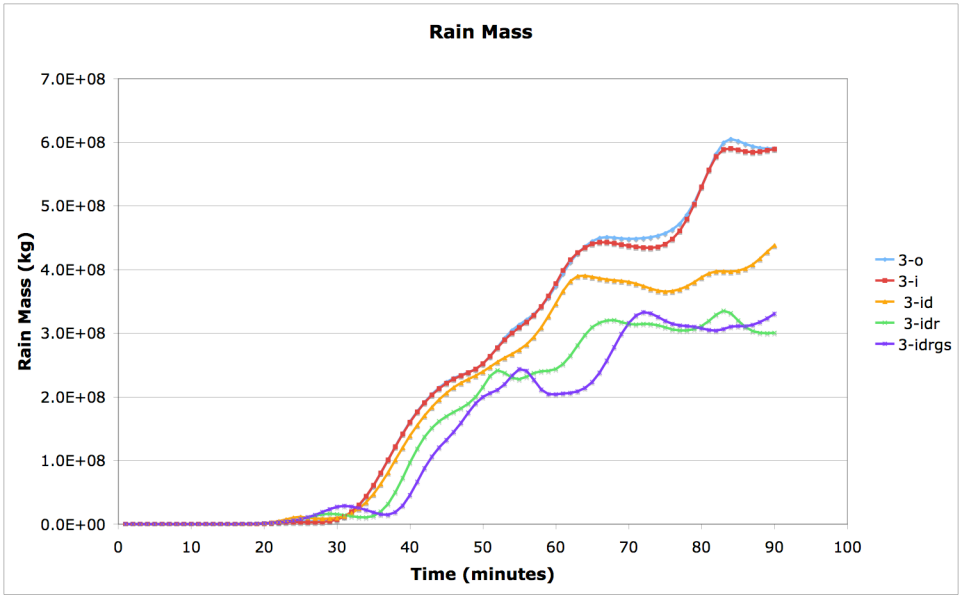

Figure 6: Total rain mass within the model domain.

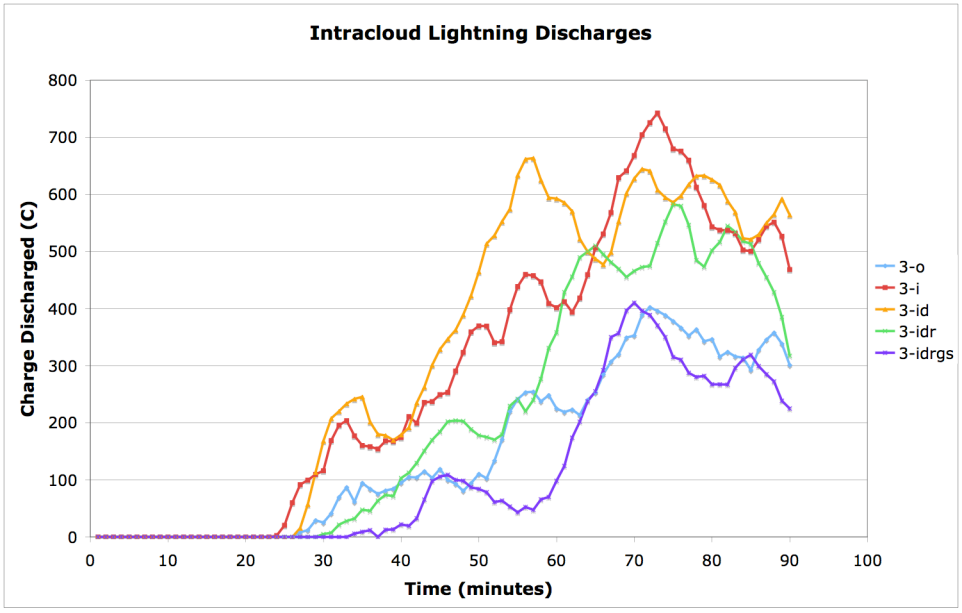

Figure 7: Total charge discharged by intracloud lightning discharges within the model domain.

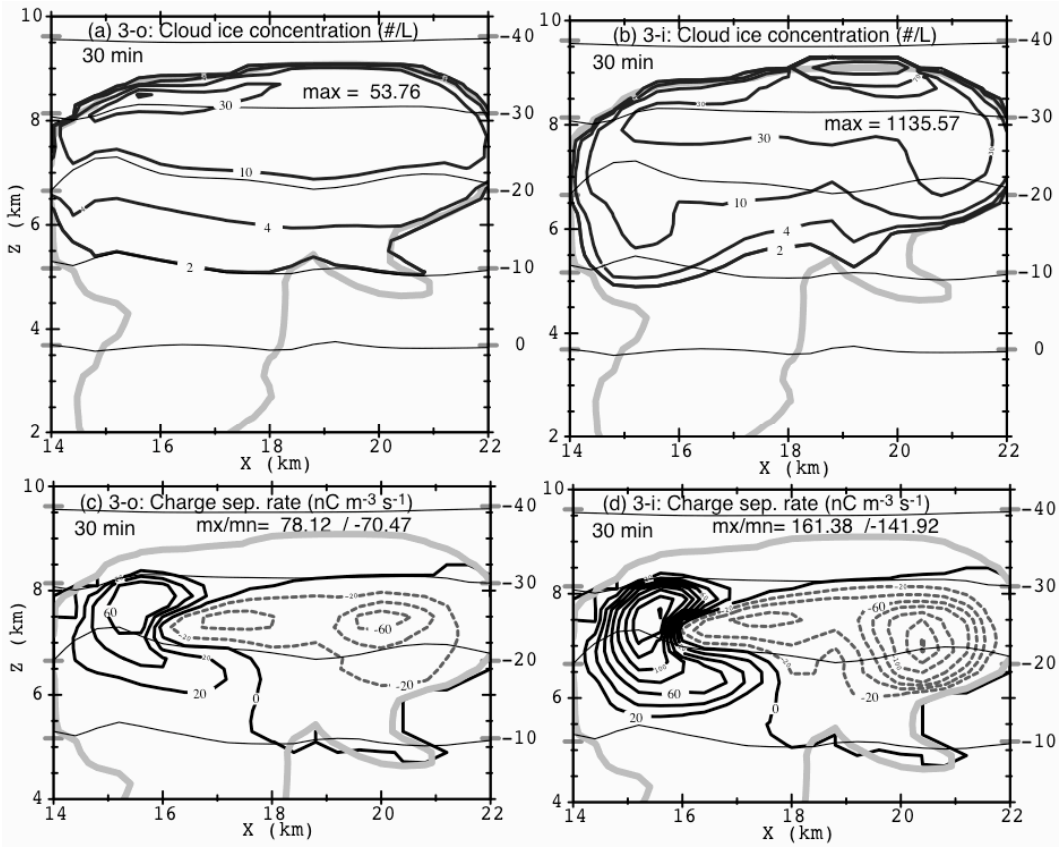

Figure 8: In (a) and (b), the cloud ice number concentrations (thick black contours) at 30 minutes are shown for runs 3-o and 3-i, respectively. In (c) and (d), the charge separation rates are shown for runs 3-o and 3-i, respectively, with areas of positive charging denoted by the thick black contours and areas of negative charging denoted by the dashed gray contours. In all cases the thin black contours are isotherms and the thick gray contours are the cloud boundary.

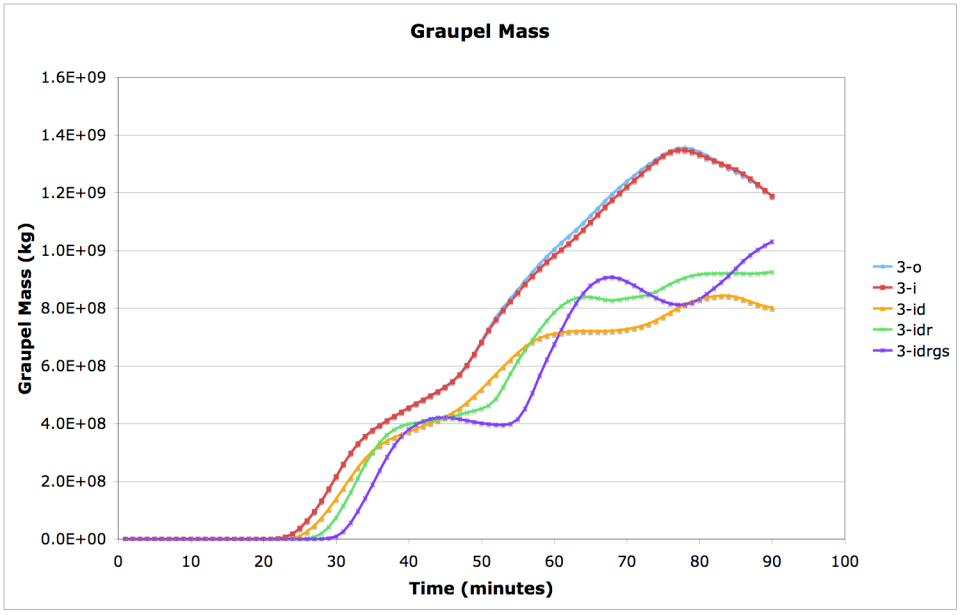

Figure 9: Total graupel mass within the model domain.

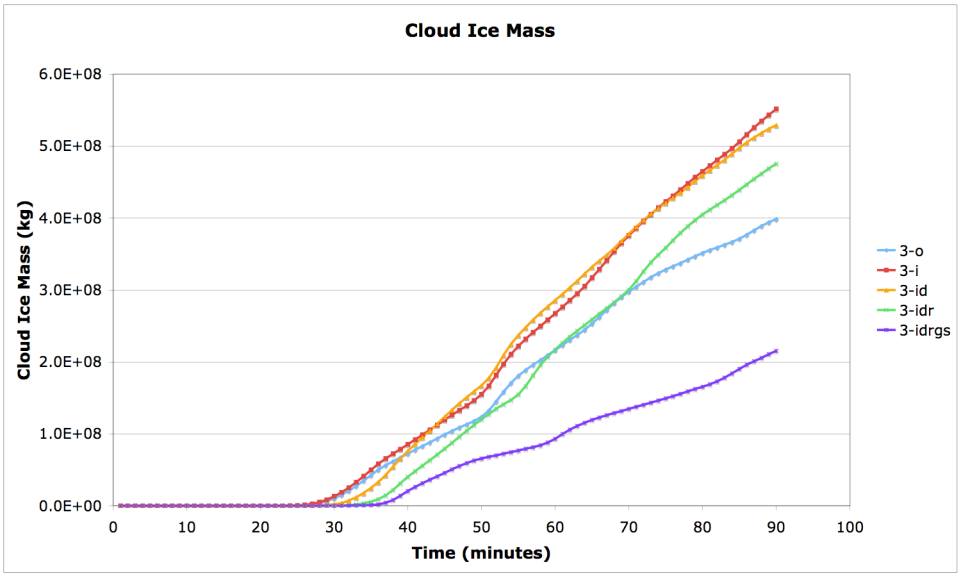

Figure 10: Total cloud ice mass within the model domain.

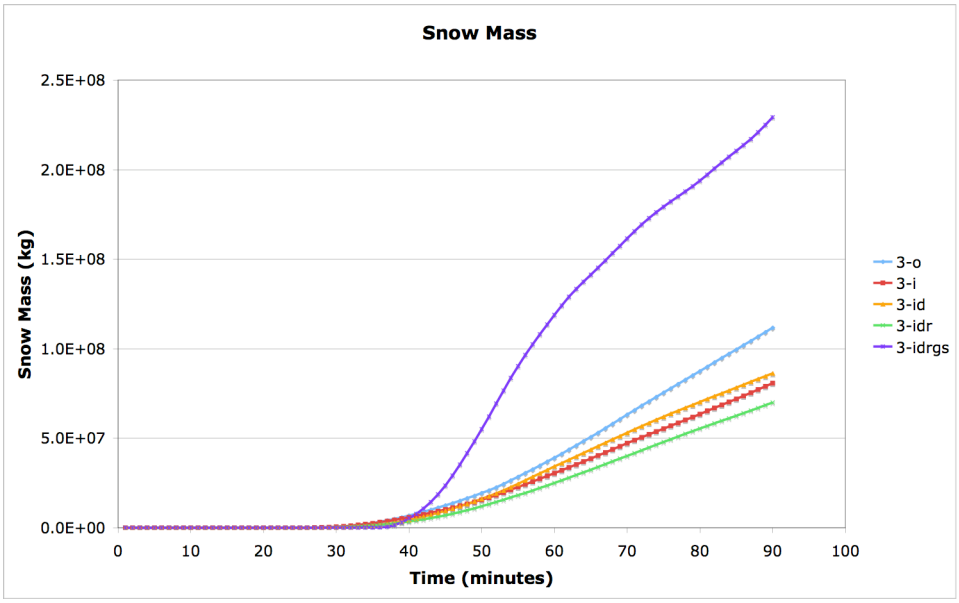

Figure 11: Total snow mass within the model domain.

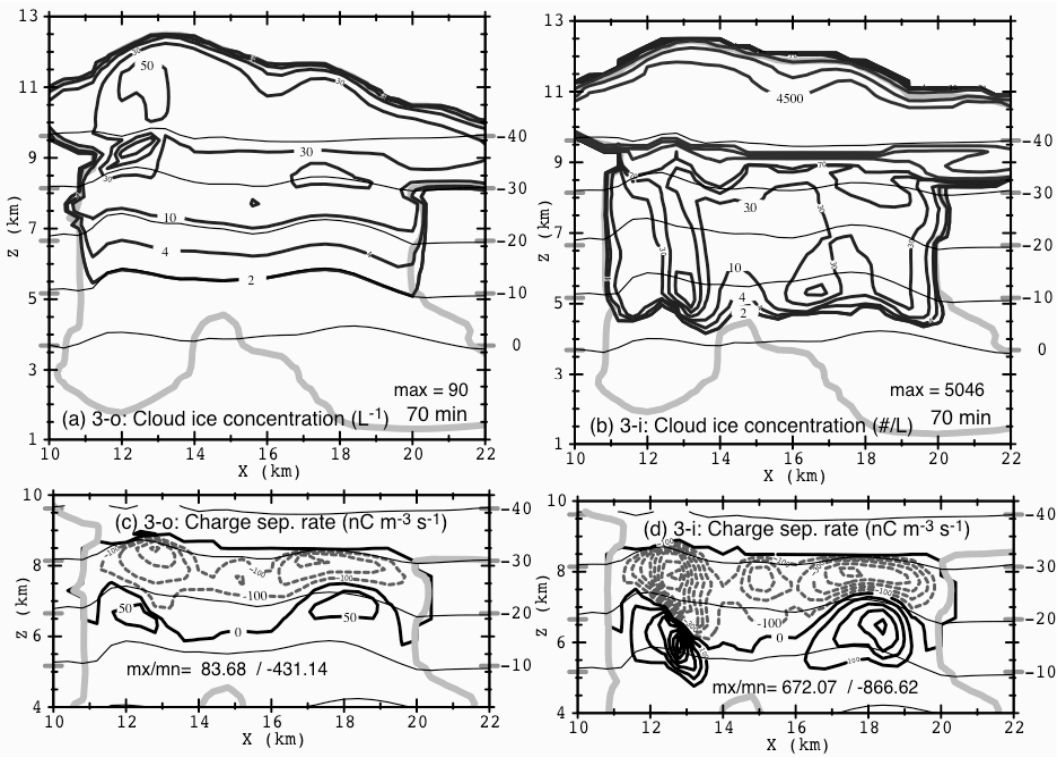

Figure 12: As in Figure 8 except at 70 minutes.